



HAL
open science

Practical PV energy harvesting under real indoor lighting conditions

Bastien Politi, Stéphanie Parola, Antoine Gademer, Diane Pegart, Marie Piquemil, Alain Foucaran, Nicolas Camara

► **To cite this version:**

Bastien Politi, Stéphanie Parola, Antoine Gademer, Diane Pegart, Marie Piquemil, et al.. Practical PV energy harvesting under real indoor lighting conditions. *Solar Energy*, 2021, 224, pp.3-9. 10.1016/j.solener.2021.05.084 . hal-03252472

HAL Id: hal-03252472

<https://hal.science/hal-03252472>

Submitted on 13 Jun 2023

HAL is a multi-disciplinary open access archive for the deposit and dissemination of scientific research documents, whether they are published or not. The documents may come from teaching and research institutions in France or abroad, or from public or private research centers.

L'archive ouverte pluridisciplinaire **HAL**, est destinée au dépôt et à la diffusion de documents scientifiques de niveau recherche, publiés ou non, émanant des établissements d'enseignement et de recherche français ou étrangers, des laboratoires publics ou privés.



Distributed under a Creative Commons Attribution - NonCommercial 4.0 International License

1 Practical PV energy harvesting under real indoor 2 lighting conditions

3 Bastien Politi^{a,b}, Stéphanie Parola^a, Antoine Gademer^{a,c}, Diane Pegart^a, Marie Piquemil^b, Alain
4 Foucaran^a, Nicolas Camara^{a,c}

5 ^a IES, University of Montpellier, CNRS, Montpellier, France

6 ^b Bureaux A Partager SAS, Paris, France

7 ^c EPF Graduate School of Engineering, Montpellier, France

8 ABSTRACT

9 Indoor light can be used as a new energy source to power μW low consumption wireless sensor
10 networks (WSNs), but for wireless electronic devices consuming tens of mW, it is still challenging.
11 The challenge comes from the low level of irradiance and from the several kinds of source
12 combinations varying in time (multi-spectral direct, reflective, and scattered mix of artificial and
13 natural light). This article describes a simple and reliable method that provides a model-based
14 evaluation of the harvestable energy from any real indoor light environment. This method uses ‘real
15 condition’ indoor light spectral measurements with a spectrometer as well as ‘controlled condition’
16 optoelectrical characteristics of the photovoltaic solar cells. The model-based evaluation of the
17 harvestable energy has been compared with real microsource prototypes based on commercial
18 photovoltaic cells powering commercial wireless e-ink display (more than 10 mW consumption
19 averaged on a day). In this article, we show that it is possible to evaluate the harvestable energy, for
20 several days of indoor light exposure, with an error lower than 6 %. Our method, with such an
21 accuracy range, will be a helpful tool to assist engineers and researchers in designing light energy
22 harvesting systems and more generally could find wide application in the growing IoT ecosystem.

24 ARTICLE INFO

25 *Keywords:* Energy Harvesting; Calculation Model; Indoor Light; Indoor PV; Mixed Light; Real Life Conditions.

26 1. Introduction

27 The number of low-power wireless devices is increasing significantly, and as a result, there is more
28 and more research focusing on new ways to supply energy to these devices (Mathúna et al., 2008).
29 Indeed, the growth in energy demand induced by this new field of application poses unprecedented
30 challenges to provide the energy needed to operate these devices (Mathews et al., 2019). It also
31 requires a review of how this energy is supplied and produced while minimizing its economic and
32 environmental impact. One practical approach investigated for this purpose is harvesting light energy
33 from the surroundings of the device. Past research has proven the viability of this approach in outdoor
34 environments (Shaikh and Zeadally, 2016). In an indoor environment, where radiated levels are low,

35 light energy harvesting has been identified as an effective method to provide enough power to low-
 36 power electronic systems such
 37 as wireless sensor networks (Matiko et al., 2014). Moreover, harvesting energy from light has
 38 demonstrated its capability as a means to achieve battery-free applications (Brunelli et al., 2009; Wang
 39 et al., 2016).

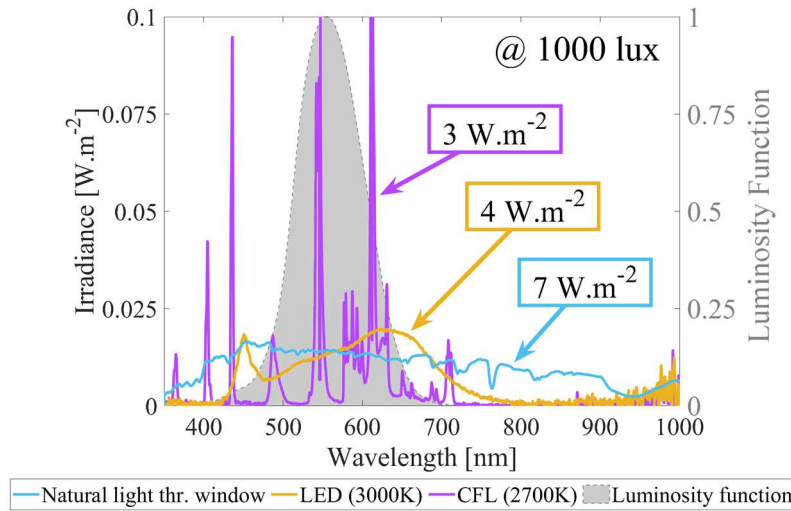
40
 41 However, when it comes to considering energy harvesting for indoor applications, the difficulty in
 42 characterizing the harvestable power becomes substantial. Even though Standard Test Conditions
 43 (STC) from IEC 60904-3 are not entirely representative of the behavior of photovoltaic (PV)
 44 converters in real-life conditions, it is still a practical way to compare them. As for indoor conditions,
 45 the situation is somewhat different. The existing standards ISO 8995:2002 and CIE S 008/E define the
 46 level of luminosity required depending on the task associated with a workplace. The unit of this
 47 appropriate luminosity level is given in a semi-empirical unit of measure called lux. The lux (or lumen
 48 per m²) value E_v is given by the following equation:

Nomenclature			
a-Si:H	hydrogenated amorphous silicon	LED	Light-Emitting Diode
CFL	compact fluorescent light	Li-Po	Lithium-Polymer
η^{SQ}	theoretical SQ solar cell efficiency	MAPE	mean absolute percentage error
η^{meas}	measured solar cell efficiency	MPPT	maximum power point tracking
E_g	bandgap energy	n	diode's ideality factor
EQE	external quantum efficiency	pc-Si	polycrystalline silicon
E_v	illuminance	PCE	power conversion efficiency (PCE)
FF^{SQ}	theoretical fill factor from SQ model	P_{in}	incident power
FF^{meas}	measured fill factor	$\Phi_{p,\lambda}$	incident photon flow
FOCV	fractional open-circuit voltage	$P^{meas}(V)$	measured power -voltage
GaAs	gallium arsenide	P_{max}^{meas}	measured maximum power
h	Planck's constant	$P^{mod}(V)$	calculated power -voltage
I_λ	irradiance	P_{max}^{mod}	calculated maximum power
J_{SC}^{SQ}	short circuit SQ current density	PMIC	power management integrated circuit
J_{SC}^{QE}	calculated short circuit current density	R_s	parasitic series resistance
J-V	current density-voltage	R_{sh}	parasitic shunt resistance
J_0^{SQ}	theoretical SQ saturation current density	SMU	Source Meter Unit
$J_{dark}^{meas}(V)$	Measured dark current density- voltage	SQ	related to Shockley-Quiesser model
J_{ph}	photocurrent density	STC	Standard Test Conditions
J_{SC}	short-circuit current density	T	photovoltaic cell temperature
$J^{mod}(V)$	estimated current density-voltage (model)	V_{OC}^{SQ}	theoretical SQ open-circuit voltage
$J^{meas}(V)$	measured current density-voltage	WSN	wireless sensor network
k	Boltzmann's constant	Y_λ	photopic luminosity function
K_{cd}	maximum spectral efficiency coefficient		

$$E_v = K_{cd} \int_0^{\infty} I_{\lambda} Y_{\lambda} d\lambda, \quad (1)$$

49 where Y_{λ} is a function related to the human eye's cones sensitivity to light (shown in Fig. 1) also called
 50 the photopic luminosity function, I_{λ} is the irradiance and K_{cd} is a coefficient called maximum spectral
 51 efficiency, defined as $686 \text{ lux}\cdot\text{W}^{-1}\cdot\text{m}^{-2}$ in such a way that irradiance of $1000 \text{ W}\cdot\text{m}^{-2}$ in standard
 52 condition (AM 1.5G) corresponds to 100 klux.

53 Nevertheless, when considering how much energy could be harvested from PV converters, the first
 54 issue arises: the luminosity in lux is not a reliable quantification of the incident harvestable power
 55 (Wang et al., 2010). Indeed, as an example, Fig. 1 presents the emission spectra from 3 different light
 56 sources: i) the natural light through a window, ii) a compact fluorescent light (CFL), and iii) a light-
 57 emitting diode (LED). The three spectra have been measured with a commercial calibrated
 58 spectroradiometer, the StellarRAD from *StellarNet Inc.*, equipped with a CR2 cosine receptor with a
 59 wavelength range from 350 nm to 1100 nm, adapted to indoor environments. Spectra are set to obtain
 60 a 1000 lux illuminance level, giving three different levels of irradiance for each light source: $7 \text{ W}\cdot\text{m}^{-2}$
 61 for natural light through the window, $3 \text{ W}\cdot\text{m}^{-2}$ for the CFL source, and $4 \text{ W}\cdot\text{m}^{-2}$ for the LED source.



62
 63 **Fig. 1.** Typical 1000 lux single source indoor environment light spectra: a 3000K LED bulb (in blue), a 2700K
 64 CFL bulb (in yellow), and natural light through a window (in red). In green, the luminosity function Y_{λ} used to
 65 establish the illuminance level (lux).

66 In addition, there is a second problem. In the case of real indoor lighting, the incident radiation is a
 67 time-varying mixture of multiple natural and artificial direct, reflective, and scattered sources: it has to
 68 be taken into account to have a reliable estimation of the photovoltaic cell performance based on real
 69 indoor light illumination (Li et al., 2015; Ma et al., 2017; Minnaert and Veelaert, 2014a; Sacco et al.,
 70 2013). Finally, the third issue is technological. Indeed, the PV converters are non-ideal devices
 71 connected to a non-ideal electrical storage device via a non-ideal power management integrated circuit
 72 (PMIC) devices. It means that the electrical energy received by the final consumer device is
 73 technology dependent and should be far from the standard theoretical Shockley-Queisser (SQ) limit

74 model predictions (Shockley and Queisser, 1961), whatever the relaxing assumption of the SQ model
 75 taken into account (Guillemoles et al., 2019). In the last few years, many researchers have been
 76 focused on overcoming these challenges to reach a reliable valuation of the harvestable surrounding
 77 low light energy, for example by optimizing the one diode photovoltaic model parameter or new
 78 experimental methods for indoor applications (Bader et al., 2019; Fajardo Jaimes and Rangel de
 79 Sousa, 2017; Ma et al., 2020; Masoudinejad et al., 2016). But in each of these studies, only the case of
 80 controlled mono artificial sources is considered.

81 In this article, we present a methodology that allows estimating the harvestable energy from any
 82 real indoor varying light environment. The first part will present a standard model based on SQ and
 83 compare it to some usual real-life PV converters. The second part will present a calculation model
 84 based on experimental data focusing mainly on a commercial flexible thin-film Gallium-Arsenide
 85 (GaAs) PV solar cell from *Alta Devices Inc.* (Kayes et al., 2011) under several controlled single
 86 sources of light. Finally, the third part will present an energy harvesting system prototype based on the
 87 GaAs solar cell, working for several days in real varying indoor environments. It is to be noted that
 88 this prototype is the micro source of a classic wireless e-ink wifi connected device, with an average
 89 power consumption of around 10 mW.

90 2. The Shockley-Queisser limit theoretical model adapted to indoor light energy harvesting

91 During the last decade, several studies have been conducted to compare the performance of different
 92 PV technologies under controlled artificial indoor light single sources (Apostolou et al., 2016;
 93 Carvalho and Paulino, 2014; De Rossi et al., 2015; Kasemann et al., 2014; Li et al., 2015; Minnaert
 94 and Veelaert, 2014b; Müller et al., 2009). Trying to face the complex task of choosing the best
 95 technology to use when dealing with indoor light-harvesting, there is an attractive approach that
 96 consists in applying the SQ limit model. This model gives the theoretical maximum conversion
 97 efficiency η^{SQ} for an ideal semiconductor single-junction solar cell at any theoretical bandgap:

$$\eta^{SQ}(E_g) = \frac{V_{OC}^{SQ} J_{SC}^{SQ} FF^{SQ}}{P_{in}}, \quad (2)$$

98 with P_{in} the incident power depending on the spectrum composition, V_{OC}^{SQ} the ideal SQ open-circuit
 99 voltage of the PV converter, J_{SC}^{SQ} the ideal SQ short circuit current and FF^{SQ} the ideal SQ fill-factor. In
 100 the case of an ideal semiconductor, the short-circuit current equals the photocurrent J_{ph}^{SQ} , which is
 101 related to the number of incident photons carrying more energy than the bandgap E_g :

$$J_{SC}^{SQ} = J_{ph}^{SQ} = q \int_0^{\lambda_g} \Phi_{p,\lambda} d\lambda, \quad (3)$$

102 Where $\Phi_{p,\lambda}$ is the incident photon flow at each optical wavelength λ , q the elementary electric
 103 charge, and λ_g the wavelength corresponding to the considered bandgap E_g .

104 The ideal SQ fill factor FF^{SQ} can be found following the semi-empirical model from Green's
 105 approximation (Green and Hall, 1982):

$$FF^{SQ} = \frac{\left[\frac{qV_{OC}^{SQ}}{kT} - \ln \left(\frac{qV_{OC}^{SQ}}{kT} + 0.72 \right) \right]}{\left(\frac{qV_{OC}^{SQ}}{kT} + 1 \right)} \quad (4)$$

106 with k being the Boltzmann's constant and T the device's temperature. The PV cell open-circuit
 107 voltage V_{OC} can be defined by the following equation, in the case of an ideality factor n equal to 1:

$$V_{OC}^{SQ} = \frac{kT}{q} \times \ln \left(\frac{J_{ph}^{SQ}}{J_0^{SQ}} + 1 \right). \quad (5)$$

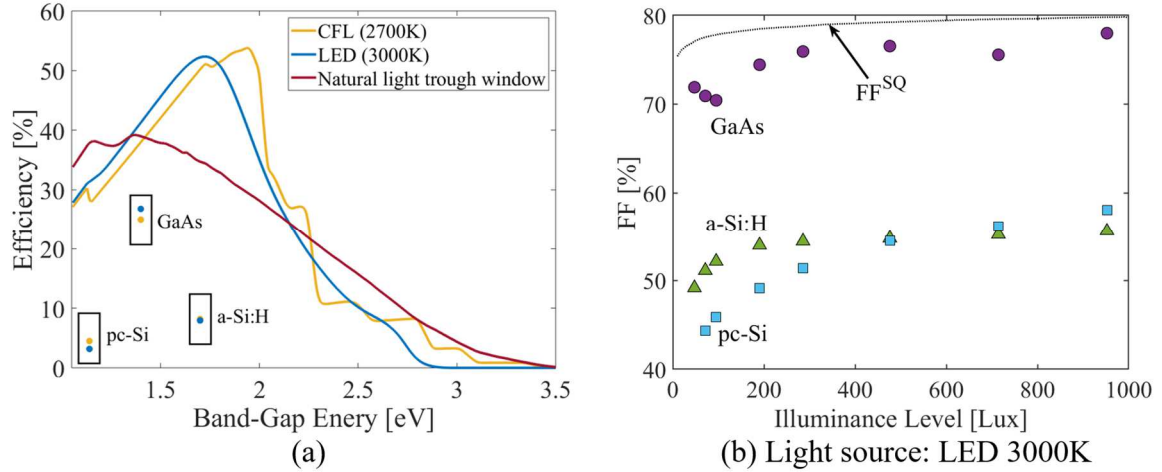
108 Finally, the ideal theoretical dark current density saturation J_0^{SQ} in a single junction is given by
 109 (Shockley and Queisser, 1961) and (Müller et al., 2013):

$$J_0^{SQ} = qA \frac{2\pi kT}{h^3 c^2} (E_g + kT)^2 e^{-\frac{E_g}{kT}} \quad (6)$$

110 with A the active surface area of the PV converter, h the Planck's constant, and c the speed of light in
 111 vacuum.

112 This SQ model is mostly known for having predicted the famous limit efficiency of 33 % for an
 113 ideal bandgap around 1.14 eV under the standard (AM 1.5G) sun radiation (Shockley and Queisser,
 114 1961). However, it can also be applied to any kind of spectra like one of the indoor light
 115 environments (Müller et al., 2013). For example, Fig. 2(a) shows the result of the SQ model when
 116 applied to typical indoor environments, identical to those in Fig. 1, each with an illuminance of 1000
 117 lux. As expected, theoretical efficiencies depend on the spectrum composition and on the fact that the
 118 ideal bandgap changes from one single source to another. As a result of this application of the SQ
 119 model, for any indoor light, the model gives theoretical efficiency much higher than the solar STC
 120 AM1.5G spectrum. In the case of a CFL source, with a theoretical semiconductor with a bandgap
 121 around $E_g = 1.95$ eV, an efficiency as high as $\eta^{SQ}(E_g) = 54$ % is predicted.

122 To compare the SQ limit theory to experimental measurement, a commercial source-meter unit
 123 (SMU), 2450 from Keithley, has been used to measure $J^{meas}(V)$: the current density-voltage
 124 characteristics of different PV converters made of different technologies: hydrogenated amorphous
 125 silicon (a-Si:H) solar cell (panel) from *Xiamen Mars Rock Science Technology Co.*, a gallium-arsenide
 126 (GaAs) mono-junction flexible PV solar cell from *Alta Devices Inc.* (Kayes et al., 2011), and a
 127 polycrystalline silicon (pc-Si) solar cell from *SEEDSTUDIO*, in controlled indoor single source
 128 environments, with different levels of irradiance. The results of the measured fill-factor FF^{meas}
 129 extracted from the $J^{meas}(V)$ curves, as well as the FF^{SQ} are plotted in Fig. 2(b).



130

131 **Fig. 2.** (a) Theoretical maximum conversion efficiency $\eta^{SQ}(E_g)$ of a single ideal p-n junction based on the SQ
 132 model for different single sources: CFL, LED, and natural light through a window. Dots are the measured
 133 efficiency of different PV converters technology under CFL and LED at around 500 lux. (b) Experimentally
 134 measured Fill-factor FF^{meas} of commercial solar cells (GaAs, a-S:H and pc-Si) and their evolution versus
 135 LED light intensity. As a comparison, an ideal solar cell FF^{SQ} based on the SQ model is shown in plain black.

136 The efficiency conversion of the different commercial PV converters technologies is, as expected,
 137 different in real conditions from what has been theoretically predicted by the SQ model. It is mostly
 138 attributed to several losses, such as shadowing, series and shunt resistance, ideality factor, optical
 139 absorption, semiconductor quality, low mobility, small minority carrier lifetime, and the PV
 140 converters' fill-factors and thus efficiencies decreasing at low light intensity (Randall and Jacot, 2003).
 141 Indeed, J_{ph}^{SQ} varies linearly with the light intensity (3), V_{OC}^{SQ} depends on J_{ph}^{SQ} (5) and FF^{SQ} depends on
 142 V_{OC}^{SQ} (4). As an example, the theoretical fill-factor based on the SQ model is shown in Fig. 2(b) for a
 143 theoretical bandgap corresponding to the standard technologies for indoor application (a-Si:H, pc-Si,
 144 and GaAs) and illuminance (from 100 to 1000 lux) with a LED single source. When comparing the
 145 experimental results of three commercial PV converters while varying the light intensity of a LED
 146 bulb, it can be seen that the fill-factor decreases with lower light intensity, as it is forecast by the
 147 theoretical FF equation, but with a more dramatic decrease. Indeed, the experimental FF^{meas} of the
 148 pc-Si cell strongly decreases when reducing the light intensity, mainly due to their too low shunt
 149 resistance (Reich et al., 2009). Thus, as reported previously and exposed in Fig. 2(b), the c-Si
 150 technology is not the most suitable technology for indoor applications, and therefore not a good
 151 candidate for developing a model based on a one-diode photovoltaic model where the FF needs to
 152 vary as little as possible. The a-Si:H and GaAs technologies have a more stable FF from 100 to 1000
 153 lux, which seems ideal for the simple model presented. Nevertheless, the FF of the a-Si:H PV
 154 converter is lower than the GaAs cell, and thus its power conversion efficiency (PCE) η^{meas} tends to
 155 indicate less promising model performance. For indoor applications, especially when dealing with

156 consumer devices with an average consumption of 10 mW, a technology that does not suffer from a
157 low level of light, but also that has a FF and a PCE close their ideal value is needed. As seen in Fig.
158 2(b), only the GaAs cells have demonstrated such good performances, with a measured FF closer to
159 the FF of the Shockley-Queisser model of an ideal solar cell than other considered cells: this is not
160 surprising since III-V solar cells are known to be among the most efficient cells, even under low
161 indoor light conditions (Mathews et al., 2016). This difference in performance is mainly due to the
162 known fact that the carrier mobility is high and the lifetime long in GaAs devices (Kayes et al., 2011),
163 that the series resistance is low enough, and the shunt resistance high enough to avoid deviation of the
164 FF , even in a low light environment. In conclusion, the fact that the experimental FF^{meas} is almost
165 constant under an illuminance ranging from 100 to 1000 lux considerably simplifies the theoretical
166 calculation of the output power of a GaAs PV cell from any spectrum, by safely applying the
167 superposition model, even at a low light intensity.

168 The next paragraph will describe a methodology based on the superposition model to predict the
169 extractable energy from the GaAs thin-film solar cell, whatever the real indoor light source
170 environment.

171 3. A calculation model of indoor light energy harvesting based on a one-diode photovoltaic model

172 The method is based on the combination of the results from three measurements: i) the light
173 environment spectrum (which is fluctuating in time), ii) the external quantum efficiency (EQE) of the
174 PV cell (unchanging intrinsic values) and iii) the measurement of the current density-voltage $J_{dark}^{meas}(V)$
175 characteristic in the dark (unchanging intrinsic values). This simple methodology allows us to consider
176 the primary deviations from the SQ model: a real EQE instead of an ideal one over the whole range of
177 the spectra, and a real $J_{dark}^{meas}(V)$ curve, which takes into account the real “shape”(FF) of the current
178 density -voltage $J(V)$ characteristic, including the parasitic series R_s and shunt R_{sh} resistances as well
179 as the ideality factor n , which can vary from 1 to 2. The spectral response was measured with a
180 custom-built setup composed of a Xenon lamp, a monochromator equipped with two diffraction
181 gratings, a filter wheel to remove the higher diffraction orders of radiation, and a lock-in amplifier. The
182 measurements were calibrated with Si and Ge photodiodes (Thorlabs FDS100-CAL and FDG03-CAL,
183 respectively) to cover the whole wavelength range of interest. This characterization does not consider
184 the impact of the solid angle of the radiation. It studies the characteristics of the PV converter with a
185 photon flow that is normal to its surface. For each wavelength band produced by the source, the current
186 generated by the characterized PV cell is measured. A known cell is used as a current-generation
187 reference to establish the EQE of the characterized PV cell by comparison.

188 In the developed model, the measured EQE is added in (3) to consider the deviation from the SQ
189 model due to the real external quantum efficiency of the PV cell. The resulting short-circuit current

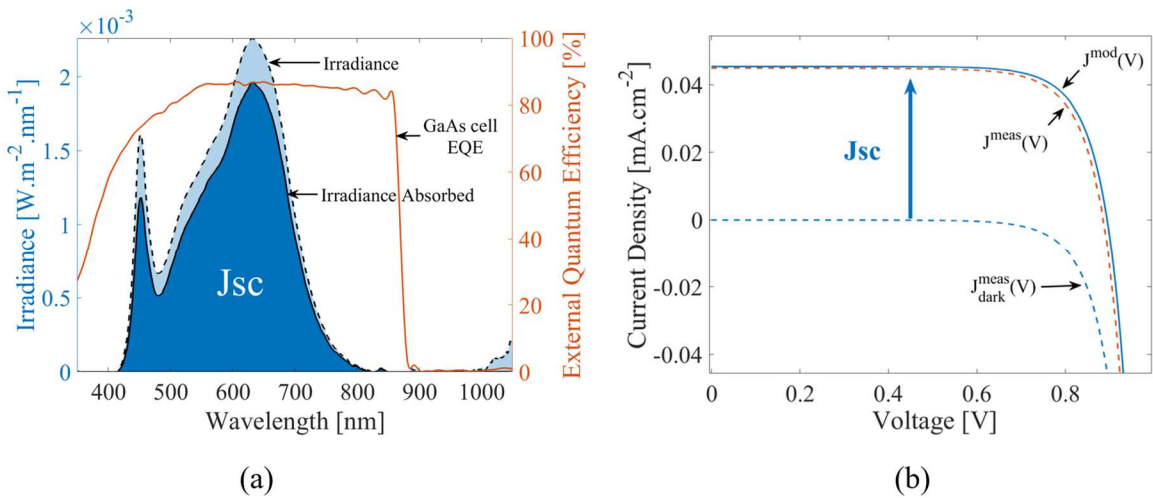
190 density J_{SC}^{QE} is thus an estimation based on two measurements: the EQE which is fixed for each PV
 191 converter and the spectra $\Phi_{p,\lambda}$ fluctuating in time:

$$J_{SC}^{QE} = q \int_0^{\lambda_g} \Phi_{p,\lambda} \times EQE \, d\lambda \quad (7)$$

192 Now that the spectral response EQE is not ideal anymore but is measured from a real solar cell, the
 193 equation (7) gives an estimated value of the short circuit density current J_{SC}^{QE} lower than in the ideal
 194 case based on the SQ model (J_{SC}^{SQ}). This value depends on the real measured spectra at any given time.
 195 Then, the measured dark current density-voltage curves $J_{dark}^{meas}(V)$ of the PV converters can be
 196 collected by the SMU 2450 from Keithley, and using the superposition principle (Lindholm et al.,
 197 1979; Tarr and Pulfrey, 1980) or more commonly known as the one-diode photovoltaic model, it is
 198 possible to deduce the estimated current density-voltage $J^{mod}(V)$ model at any given time of the
 199 fluctuating spectra:

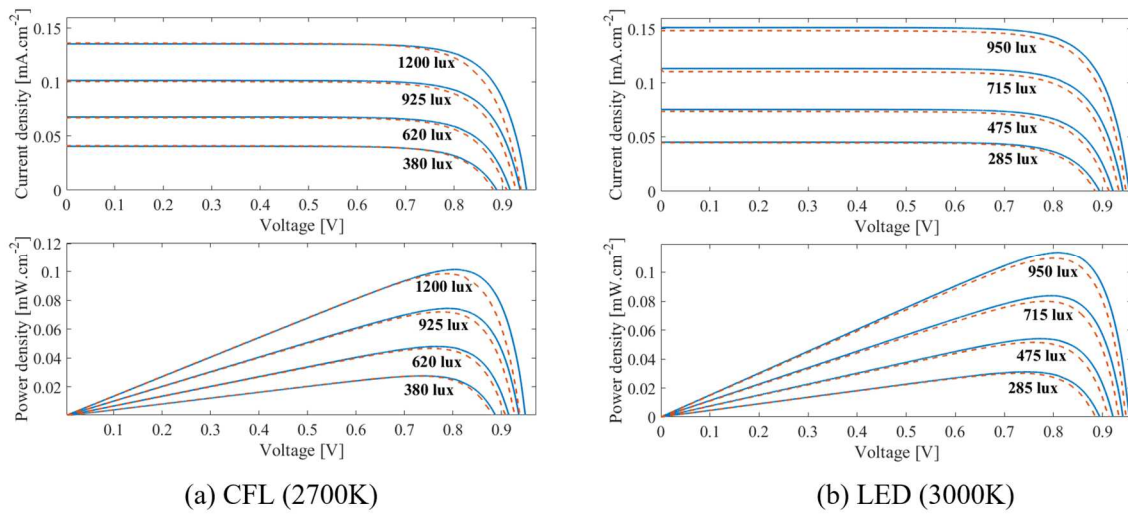
$$J^{mod}(V) = J_{dark}^{meas}(V) + J_{SC}^{QE} \quad (8)$$

200 As an example, Fig. 3(a) shows the LED spectra of a 300 lux LED 3000K bulb as well as the
 201 measured EQE curve of a GaAs solar cell and the current generation of this cell resulting from its
 202 absorption of the photon flux. In Fig. 3(b), based on the previous EQE curve and the LED spectra and
 203 the $J_{dark}^{meas}(V)$ curve, the estimated $J^{mod}(V)$ is shown as well as the measured $J^{meas}(V)$. In this first
 204 example, the current density curve $J^{mod}(V)$, estimated from the developed model, is in good
 205 agreement with the experimentally measured $J^{meas}(V)$. In this example, the extracted maximal power
 206 values P_{max}^{mod} and P_{max}^{meas} from the model $J^{mod}(V)$ and measured $J^{meas}(V)$, are $30 \mu\text{W}/\text{cm}^2$ and
 207 $31 \mu\text{W}/\text{cm}^2$, respectively, with a difference of about 3 %.



208 (a)
 209 **Fig.3.** (a) spectra of a 300 lux LED 3000K bulb and the same spectra modulated by the measured external
 210 quantum efficiency of a GaAs solar cell. (b) the $J_{dark}^{meas}(V)$ curve of the GaAs solar cell in blue dash used to
 211 calculate the expected $J^{mod}(V)$ based on (8) in orange dash, compared to the experimentally measured $J^{meas}(V)$.

212 We have used this method with the same GaAs solar cell under single controlled sources light
 213 environments, for different sources (CFL and LED) at many different levels of indoor irradiance (from
 214 200 lux up to 1000 lux), to verify the reliability of the one-diode photovoltaic model. The
 215 characteristics resulting from the model, $J^{mod}(V)$ and the $P^{mod}(V)$, are shown in Fig. 4 and compared
 216 to their experimental equivalents, $J^{meas}(V)$ and the $P^{meas}(V)$. The deviation between model results
 217 and the experimental measurements is noticeable but minor. With an average error of less than 3 %
 218 and never exceeding 5 %, considering the numerous experimental bias possible, these results seem
 219 sufficiently accurate to be useful for the calculation of a harvestable power approximation in various
 220 low irradiance indoor environments.



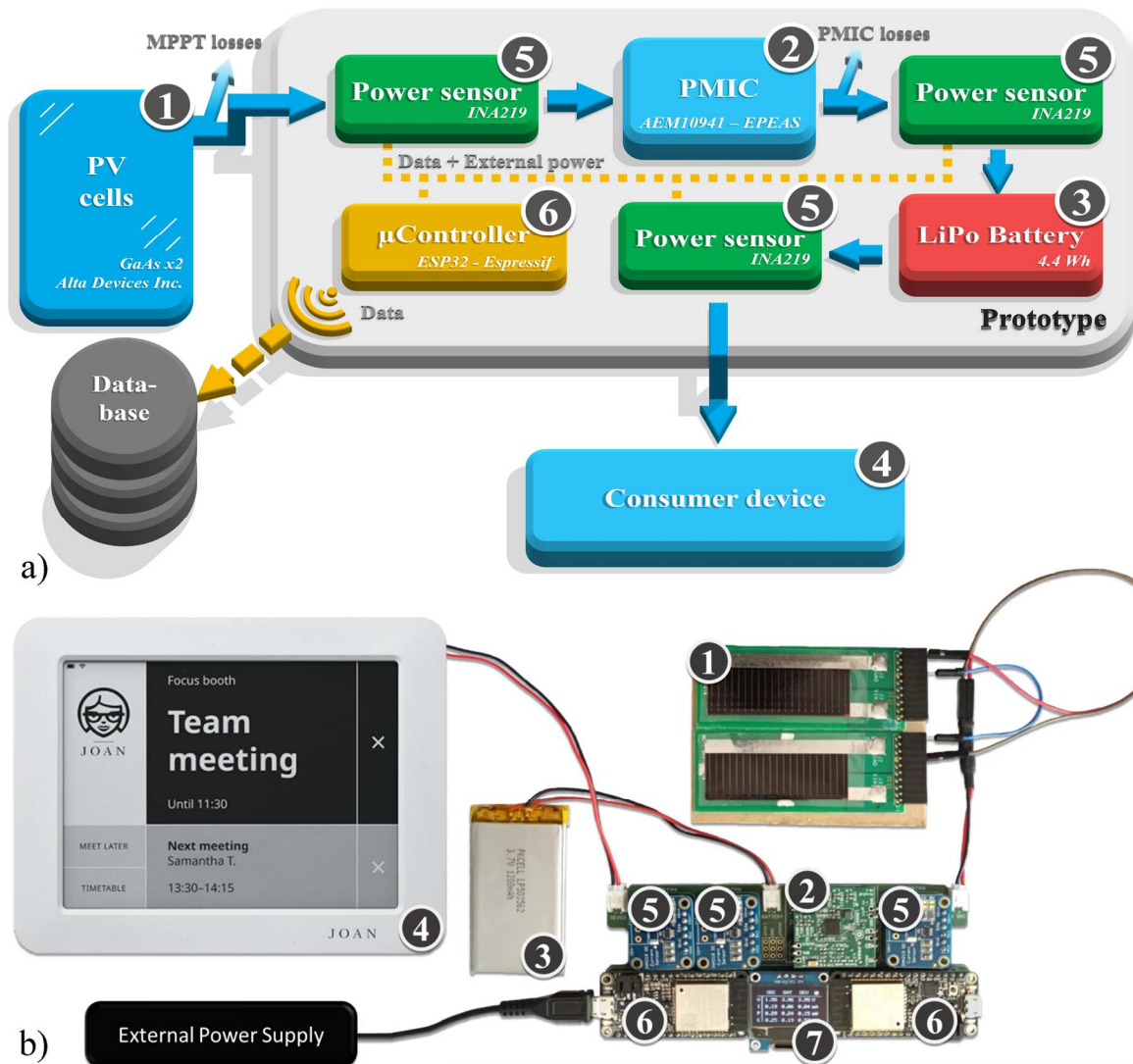
221 (a) CFL (2700K) (b) LED (3000K)
 222 **Fig. 4** Comparison between the calculated J^{mod} -V and the P^{mod} -V (plain blue lines) from the one-diode
 223 photovoltaic model and the corresponding experimental characteristics J^{meas} -V and the P^{meas} -V (dotted orange
 224 lines) of a GaAs solar cell for different illuminance under (a) a CFL light source and (b) a LED light source.

225 As stated previously in this paper, the lack of standards to rely on makes studying in the field of
 226 indoor PV more complex. Consequently, it is necessary to find a method to evaluate the produced
 227 energy based on the analysis of a fluctuating mix of natural and artificial light environments. The next
 228 paragraph will demonstrate the reliability of the simple one-diode photovoltaic model described
 229 beforehand to calculate the harvestable energy in real-life indoor conditions, even for several days.

230 4. The model applied in real conditions for several days

231 The ultimate purpose of this study is to establish a model to calculate, as precisely as possible, the
 232 level of harvestable energy in a real indoor environment for an extended period. Therefore, it is
 233 necessary to test the model under real-life conditions, observing the light environment over time to
 234 know the variations in its composition and to compare the calculated results to experimental results. A
 235 complete energy harvesting prototype, shown in Fig. 5, has been developed to validate the developed
 236 model experimentally in real-life environments. This prototype is based on two GaAs thin-film solar
 237 cells providing electrical energy to the energy storage device (here a Lithium-Polymer battery) of a

238 consumer device like an e-ink connected device. To extract the maximum power from the solar cells, a
 239 very low consumption commercial power management integrated circuit (PMIC) from *e-PEAS* has
 240 been placed between the PV cells and the LiPo battery.



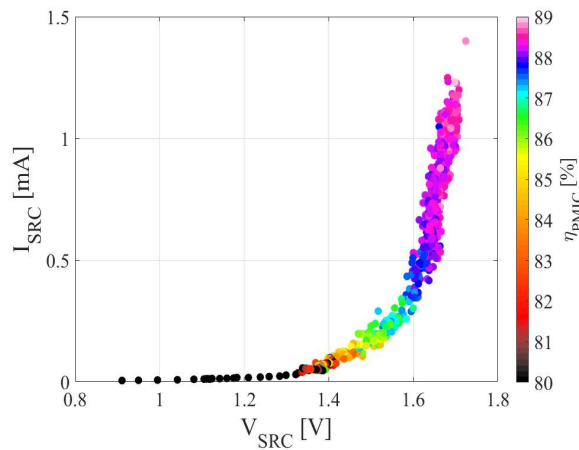
241
 242 **Fig. 5. a)** Schematic of the energy harvesting prototype (PV cells + PMIC + LiPo battery) that has been
 243 instrumented by three INA 219 electrical power sensors and two ESP32 microchips to collect the data and send
 244 them to a database. Let's note there is a specific external power source that allows the acquisition and
 245 transmission of data without affecting the performance of the energy harvester. b) a picture of the described
 246 prototype integrating GaAs solar cells (1), a PMIC : an *e-peas* 'EVK10941M' Mini Evaluation Board based on
 247 the 'AEM10941' Solar Energy Harvesting IC (2); a LiPo electrical storage device (3), the e-ink communicating
 248 device to power (4), the INA219 power sensors (5), the ESP32 low cost low power microcontroller chips (6) and
 249 an OLED screen (7).

250 The used PMIC is based on a max power point tracking (MPPT) algorithm called fractional open-
 251 circuit voltage (FOCV). This method relies on getting a sample of the V_{oc} and then applies and holds a
 252 fraction of its value to the PV cells or module (Motahhir et al., 2020). Besides not being the most
 253 performant in casual energy harvesting situations, such an MPPT algorithm has demonstrated its use of
 254 relevance in low light environments (Weddell et al., 2012). Even though this PMIC is adapted for low

255 energy harvesting applications, the losses are not negligible. To include these losses in our model, and
 256 to be able to measure the “real” power harvested by the prototype at any time into the LiPo battery,
 257 two voltage and current sensing chips INA219 from *Texas Instrument* have been inserted between the
 258 PV cells and the PMIC and between the PMIC and the LiPo. Regarding the classical Lithium Polymer
 259 (LiPo) battery whom internal resistance is usually less than $100\text{m}\Omega$, it has no impact in term of losses
 260 when considering the low current level in our application. In addition, a third INA219 has been
 261 inserted between the LiPo battery and the consumer device to monitor its consumption. A set of two
 262 microcontrollers associated with these power sensors allows the acquisition of the power
 263 generation/consumption data from the three INA 219, and their recording on a database in the cloud.
 264 An external power source is used to power the sensors and the microcontrollers.

265

266 The e-peas PMIC Mini Evaluation Board EVK10941M chosen for the prototype uses the fractional
 267 open-circuit voltage (FOCV) algorithm. To extract the maximum power from the PV cells, this PMIC
 268 algorithm can be configured to apply 70%, 75%, 85%, or 90% of their V_{oc} . In our application, by
 269 choosing the fraction of 85%, the MPPT losses due to the optimal fraction of V_{oc} not being exactly
 270 equal to 85%, are evaluated to be lower than 1% over the whole range of illumination. Regarding the
 271 PMIC losses induced by the classical losses of a buck-boost converter, they can vary from 10% to 20%
 272 depending on the level of illumination. As can be seen in Fig.6, at low light (and low V_{SRC} et low I_{SRC}),
 273 the efficiency of the PMIC is only 80 % while at moderate to high illumination the efficiency is about
 274 90%. From the plot of Fig.6, a regressive equation has been added to our model to include the PMIC
 275 efficiency η^{PMIC} .

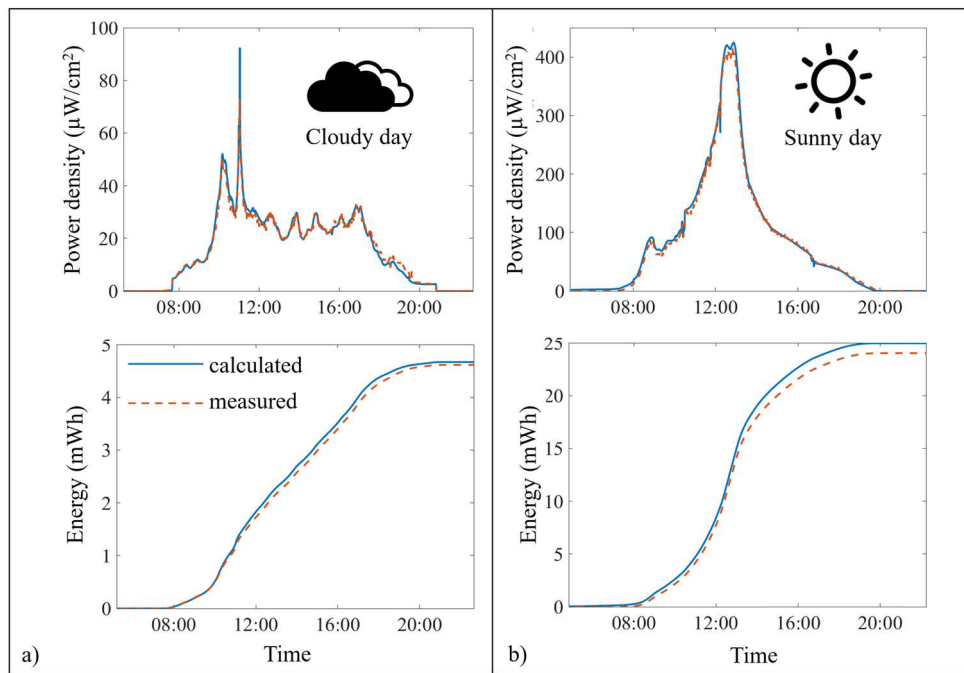


276

277 *Fig. 6. Experimental PMIC efficiency η^{PMIC} depending on ligh intensity. These curve depends on the*
 278 *experimental set-up , in our case two GaAs solar cell in series , an epeas based PMIC and a single cell LiPo.*

279 Finally, the purpose of the experiment is to compare the harvestable energy calculated by the model
 280 and the real harvested energy measured by the power sensor, the power measurements must be carried
 281 out simultaneously with the spectrometer analysis of the light environment to which the prototype is
 282 exposed. This experiment has been carried out over 21 days. The results of 2 typical days (sunny and

283 cloudy days) are shown in Fig.7. While the orange dashed line is the experimental harvested power
 284 stored into the Lithium Polymer battery measured directly by an INA219, the blue line represents the
 285 model calculation results based on one-minute spectra measurement intervals. A qualitative agreement
 286 between the model calculation of power and energy harvesting and the real usable power generated
 287 and energy transferred to the prototype battery can be observed. The mean absolute percentage error
 288 (MAPE) between the model curve and the experimental power curve of each of the 21 days is lower
 289 than 6%. These very good results are comforting the fact that our model and methods are reliable
 290 enough to be an interesting tool for researchers and engineers conceiving indoor micro source elements
 291 for IoT applications or consumer devices.



292
 293
 294 **Fig. 7.** model's power density and energy calculations (plain blue) and experimentally measured power-density
 295 and energy (dash orange) generated from the GaAs solar cell in a real-life indoor environment harvested into the
 296 Lithium Polymer storage device for a) a cloudy day and b) a sunny day.

297 The 6% of error are potentially due to several factors: i) the MPPT losses ii) the LiPo battery losses,
 298 iii) the reliability of the low-cost INA219, iv) the reliability of our model which has been taken as
 299 simple as possible without taking into account potential variation of R_{sh} and R_s with light intensity,
 300 v) the small effect of temperature in indoor Environment, vi) and of course the experimental setup.

301
 302 These results obtained after 21 days of observation of the office's real lighting environment show
 303 that the model makes it possible to determine the level of harvestable energy per surface unit quite
 304 accurately, even if there is still room for improvement. It is then possible to determine, based on these
 305 21 days of observation, the harvesting surface area or the number of PV cells required in this
 306 environment to compensate for the energy needs of an electronic device fully. For example, a classical

307 wireless e-ink dashboard, as the one used in this study, depending on its size and the significance of its
308 sleeping mode, consumes about 10 mW on average. In such a case, a preliminary extrapolation shows
309 that 14x14 cm² of similar solar cells would be sufficient to supply it enough power to make it
310 energetically autonomous.

311 **5. Conclusion**

312 In summary, the simple model presented applying the superposition principle, based on the
313 combination of the measured optical EQE and electrical J_{dark}^{meas} -V of GaAs PV cell in the dark,
314 combined with the spectral measurements of real-life indoor environments, has demonstrated the
315 ability to calculate the potentially harvestable energy in the environment that is being studied. Using
316 an energy-harvesting prototype installed in the environment studied by the spectrometer feeding the
317 developed model allowed to confront results from the model to actual power and energy harvest. The
318 confrontation result corroborates the ability of the proposed model to calculate the harvestable energy
319 with an error lower than 6 % for the 21 days of the test. In a more practical sense, this paper shows
320 that in real-life indoor environments, a module based on PV cells similar to *Alta Devices Inc.* GaAs
321 PV solar cells and smaller than a third of a sheet of paper (A4 format) is enough to make devices
322 consuming about 10 mW.

323 We believe that the method presented in this article will be helpful to engineers and researchers
324 attempting to overcome the various challenges toward the accurate design of energy harvesting
325 devices in the future.

326 **Declaration of Competing Interest**

327 The authors declare no conflict of interest.

328 **Acknowledgments**

329 This work has been funded by the French national association for research and technology (ANRT)
330 [grant CIFRE number 2017/0331].

331 **References**

- 332 Apostolou, G., Reinders, A., Verwaal, M., 2016. Comparison of the indoor performance of 12 commercial PV
333 products by a simple model. *Energy Sci. Eng.* 4, 69–85. <https://doi.org/10.1002/ese3.110>
- 334 Bader, S., Ma, X., Oelmann, B., 2019. One-diode photovoltaic model parameters at indoor illumination levels –
335 A comparison. *Sol. Energy* 180, 707–716. <https://doi.org/10.1016/j.solener.2019.01.048>
- 336 Brunelli, D., Moser, C., Thiele, L., Benini, L., 2009. Design of a solar-harvesting circuit for batteryless
337 embedded systems. *IEEE Trans. Circuits Syst. I Regul. Pap.* 56, 2519–2528.
338 <https://doi.org/10.1109/TCSI.2009.2015690>
- 339 Carvalho, C., Paulino, N., 2014. On the Feasibility of Indoor Light Energy Harvesting for Wireless Sensor
340 Networks. *Procedia Technol.* 17, 343–350. <https://doi.org/10.1016/j.protcy.2014.10.206>
- 341 De Rossi, F., Pontecorvo, T., Brown, T.M., 2015. Characterization of photovoltaic devices for indoor light
342 harvesting and customization of flexible dye solar cells to deliver superior efficiency under artificial
343 lighting. *Appl. Energy* 156, 413–422. <https://doi.org/10.1016/j.apenergy.2015.07.031>
- 344 Fajardo Jaimes, A., Rangel de Sousa, F., 2017. Simple modeling of photovoltaic solar cells for indoor harvesting
345 applications. *Sol. Energy* 157, 792–802. <https://doi.org/10.1016/j.solener.2017.08.077>

346 Green, M.A., Hall, P., 1982. Solar cells—Operating principles, technology and system applications. *Sol. Energy*
347 28, 447. [https://doi.org/10.1016/0038-092x\(82\)90265-1](https://doi.org/10.1016/0038-092x(82)90265-1)

348 Guillemoles, J.F., Kirchartz, T., Cahen, D., Rau, U., 2019. Guide for the perplexed to the Shockley–Queisser
349 model for solar cells. *Nat. Photonics* 13, 501–505. <https://doi.org/10.1038/s41566-019-0479-2>

350 Kasemann, M., Kokert, J., Torres, S.M., Ruhle, K., Reindl, L.M., 2014. Monitoring of indoor light conditions for
351 photovoltaic energy harvesting, in: 2014 IEEE 11th International Multi-Conference on Systems, Signals
352 and Devices, SSD 2014. <https://doi.org/10.1109/SSD.2014.6808770>

353 Kayes, B.M., Nie, H., Twist, R., Spruytte, S.G., Reinhardt, F., Kizilyalli, I.C., Higashi, G.S., 2011. 27.6%
354 Conversion efficiency, a new record for single-junction solar cells under 1 sun illumination. *Conf. Rec.*
355 *IEEE Photovolt. Spec. Conf.* 000004–000008. <https://doi.org/10.1109/PVSC.2011.6185831>

356 Li, Y., Grabham, N.J., Beeby, S.P., Tudor, M.J., 2015. The effect of the type of illumination on the energy
357 harvesting performance of solar cells. *Sol. Energy* 111, 21–29.
358 <https://doi.org/10.1016/j.solener.2014.10.024>

359 Lindholm, F.A., Fossum, J.G., Burgess, E.L., 1979. Application of the superposition principle. *IEEE Trans.*
360 *Electron Devices* 26, 165–171. <https://doi.org/10.1119/1.2343232>

361 Ma, X., Bader, S., Oelmann, B., 2020. Power Estimation for Indoor Light Energy Harvesting Systems. *IEEE*
362 *Trans. Instrum. Meas.* 9456, 1–1. <https://doi.org/10.1109/tim.2020.2984145>

363 Ma, X., Bader, S., Oelmann, B., 2017. Characterization of indoor light conditions by light source classification.
364 *IEEE Sens. J.* 17, 3884–3891. <https://doi.org/10.1109/JSEN.2017.2699330>

365 Masoudinejad, M., Kamat, M., Emmerich, J., Ten Hompel, M., Sardesai, S., 2016. A gray box modeling of a
366 photovoltaic cell under low illumination in materials handling application. *Proc. 2015 IEEE Int. Renew.*
367 *Sustain. Energy Conf. IRSEC 2015.* <https://doi.org/10.1109/IRSEC.2015.7455081>

368 Mathews, I., Kantareddy, S.N., Buonassisi, T., Peters, I.M., 2019. Technology and Market Perspective for Indoor
369 Photovoltaic Cells. *Joule* 3, 1415–1426. <https://doi.org/10.1016/j.joule.2019.03.026>

370 Mathews, I., King, P.J., Stafford, F., Frizzell, R., 2016. Performance of III – V Solar Cells as Indoor Light
371 Energy Harvesters. *IEEE J. Photovoltaics* 6, 230–235. <https://doi.org/10.1109/JPHOTOV.2015.2487825>

372 Mathúna, C.Ó., O'Donnell, T., Martínez-Catala, R. V., Rohan, J., O'Flynn, B., 2008. Energy scavenging for
373 long-term deployable wireless sensor networks. *Talanta* 75, 613–623.
374 <https://doi.org/10.1016/j.talanta.2007.12.021>

375 Matiko, J.W., Grabham, N.J., Beeby, S.P., Tudor, M.J., 2014. Review of the application of energy harvesting in
376 buildings. *Meas. Sci. Technol.* 25. <https://doi.org/10.1088/0957-0233/25/1/012002>

377 Minnaert, B., Veelaert, P., 2014a. A proposal for typical artificial light sources for the characterization of indoor
378 photovoltaic applications. *Energies* 7, 1500–1516. <https://doi.org/10.3390/en7031500>

379 Minnaert, B., Veelaert, P., 2014b. The Potential of Tandem Photovoltaic Solar Cells for Indoor Applications 1–
380 10.

381 Motahhir, S., El Hammoumi, A., El Ghzizal, A., 2020. The most used MPPT algorithms: Review and the
382 suitable low-cost embedded board for each algorithm. *J. Clean. Prod.* 246.
383 <https://doi.org/10.1016/j.jclepro.2019.118983>

384 Müller, M., Wienold, J., Walker, W.D., Reindl, L.M., 2009. Characterization of indoor photovoltaic devices and
385 light, in: *Conference Record of the IEEE Photovoltaic Specialists Conference.* pp. 000738–000743.
386 <https://doi.org/10.1109/PVSC.2009.5411178>

387 Müller, M.F., Freunek, M., Reindl, L.M., 2013. Maximum efficiencies of indoor photovoltaic devices. *IEEE J.*
388 *Photovoltaics* 3, 59–64. <https://doi.org/10.1109/JPHOTOV.2012.2225023>

389 Randall, J.F., Jacot, J., 2003. Is AM1.5 applicable in practice? Modelling eight photovoltaic materials with
390 respect to light intensity and two spectra. *Renew. Energy* 28, 1851–1864. [https://doi.org/10.1016/S0960-1481\(03\)00068-5](https://doi.org/10.1016/S0960-1481(03)00068-5)

391

392 Reich, N.H., van Sark, W.G.J.H.M., Alsema, E.A., Lof, R.W., Schropp, R.E.I., Sinke, W.C., Turkenburg, W.C.,
393 2009. Crystalline silicon cell performance at low light intensities. *Sol. Energy Mater. Sol. Cells* 93, 1471–
394 1481. <https://doi.org/10.1016/j.solmat.2009.03.018>

395 Sacco, A., Rolle, L., Scaltrito, L., Tresso, E., Pirri, C.F., 2013. Characterization of photovoltaic modules for low-
396 power indoor application. *Appl. Energy* 102, 1295–1302. <https://doi.org/10.1016/j.apenergy.2012.07.001>

397 Shaikh, F.K., Zeadally, S., 2016. Energy harvesting in wireless sensor networks: A comprehensive review.
398 *Renew. Sustain. Energy Rev.* 55, 1041–1054. <https://doi.org/10.1016/j.rser.2015.11.010>

399 Shockley, W., Queisser, H.J., 1961. Detailed balance limit of efficiency of p-n junction solar cells. *J. Appl. Phys.*
400 32, 510–519. <https://doi.org/10.1063/1.1736034>

401 Tarr, N.G., Pulfrey, D.L., 1980. The Superposition Principle for Homojunction Solar Cells. *IEEE Trans. Electron*
402 *Devices* 27, 771–776. <https://doi.org/10.1109/T-ED.1980.19935>

403 Wang, W.S., O'Donnell, T., Wang, N., Hayes, M., O'Flynn, B., O'Mathuna, C., 2010. Design considerations of
404 sub-mw indoor light energy harvesting for wireless sensor systems. *ACM J. Emerg. Technol. Comput.*
405 *Syst.* 6. <https://doi.org/10.1145/1773814.1773817>

- 406 Wang, Y., Liu, Y., Wang, C., Li, Z., Sheng, X., Lee, H.G., Chang, N., Yang, H., 2016. Storage-Less and
407 Converter-Less Photovoltaic Energy Harvesting with Maximum Power Point Tracking for Internet of
408 Things. *IEEE Trans. Comput. Des. Integr. Circuits Syst.* 35, 173–186.
409 <https://doi.org/10.1109/TCAD.2015.2446937>
- 410 Weddell, A.S., Merrett, G. V., Al-Hashimi, B.M., 2012. Photovoltaic sample-and-hold circuit enabling MPPT
411 indoors for low-power systems. *IEEE Trans. Circuits Syst. I Regul. Pap.* 59, 1196–1204.
412 <https://doi.org/10.1109/TCSI.2011.2173393>